

## **Limited-aperture CSP gathers used for AVO analysis**

Shuang Sun and John C. Bancroft

### **ABSTRACT**

Traditionally amplitude variation with offset (AVO) is performed on CMP gathers on prestack data. However even if the subsurface has a mild structure, the common mid-point is no longer the common depth point. Thus AVO analysis after prestack migration is desired. The formation of the common-scatterpoint (CSP) gather provides a useful tool for such method.

### **METHOD**

#### **Cheops' pyramid and Specular energy**

In seismic modelling an event may be constructed from a series of scatterpoints. Using a 2-D zero-offset forward model  $(x,t)$  the scatterpoints can be modelled by spreading energy on hyperbolas, the shape of which is defined by RMS velocity at the scatterpoint. Prestack modelling uses 3D surface of Cheops' pyramid to recreate the reflection surface in  $(x,h,t)$ . The prestack data  $(x,h,t)$  for a 2D line can be modelled by spreading energy in this volume with the shape of Cheops' pyramid defined by RMS velocity at the scatterpoint.

#### *Modelling a horizontal reflector*

Figure 1 shows a horizontal hyperbolic cylinder that represents the hyperbolic moveout from a horizontal reflector in a constant velocity medium. Below the hyperbolic cylinder is a Cheops' pyramid formed from one scatterpoint that lies on the horizontal reflector. The Cheops' pyramid is tangential to the hyperbolic cylinder at constant  $x$ , or at the CMP gather that passes through the scatterpoint.

The hyperbolic cylinder can be considered a reconstruction of many Cheops' pyramids from many horizontal scatterpoints. In Figures 1a - b, the Cheops' pyramid has had the time reduced by a small fraction, so that it will protrude through the hyperbolic cylinder, to illustrate the area of tangency. This area of tangency is visible in (b), surrounding the CMP gather located at the scatterpoint.

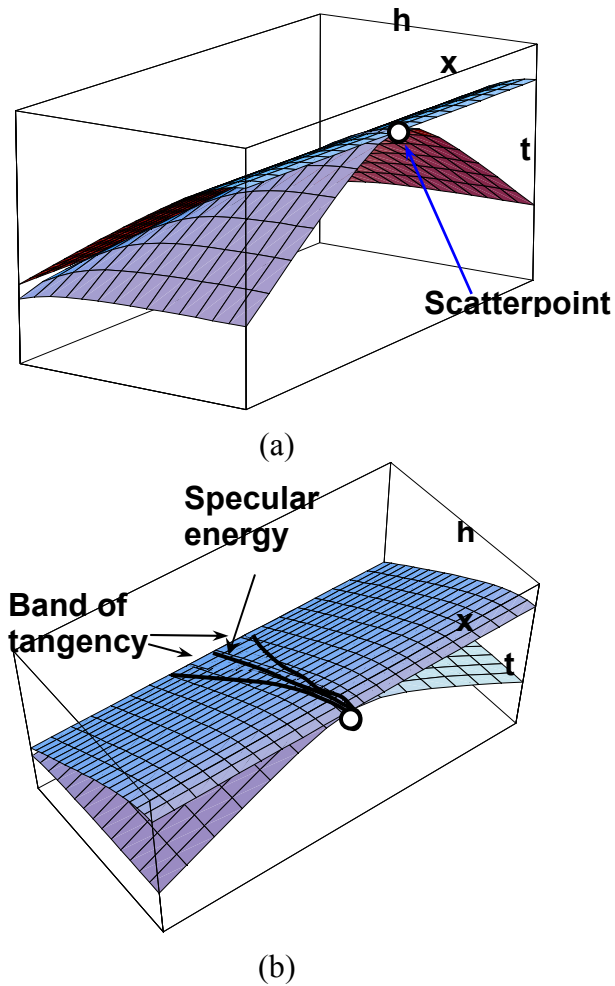


FIG 1. Two perspective views a) and b) of pre-stack surface from a horizontal reflector with a scatterpoint and Cheops' pyramid (From Bancroft, 1999).

### *Modelling a dipping event*

A 2D dipping event, illustrated in the ray tracing of Figure 2, may be modelled in the pre-stack volume  $(x, h, t)$ , to produce the surface in Figure 2a. This surface is exactly hyperbolic in each CMP gather. Dip-dependent moveout (DD-MO) corrects offset time in CMP gathers to a zero-offset time; however the actual offset reflection points should move updip from this CMP gather (Figure 2a).

In a manner similar to 2D diffraction modelling, the pre-stack hyperbolic surface of Figure 2a may also be modelled by a reconstruction of Cheops' pyramids, formed from a series of scatterpoints that are located along the dipping event, as illustrated by one scatterpoint in Figure 2b.

Figure 2b shows various offset raypaths for a single reflecting point on the dipping event. As CMP moves away from the reflecting point, the distance on the surface between CMP and the reflecting point becomes larger. Their midpoints are identified by the black dots. As the offset is increased, the midpoint of each source/receiver moves down dip.

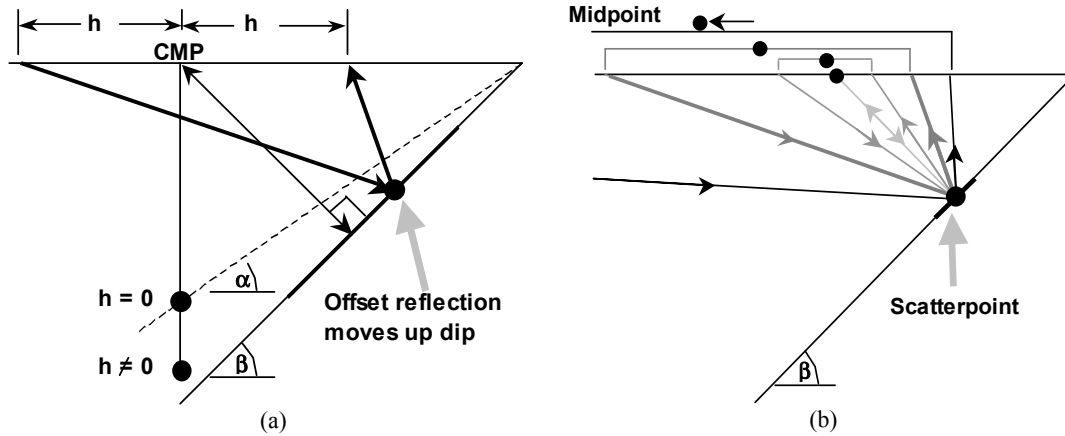
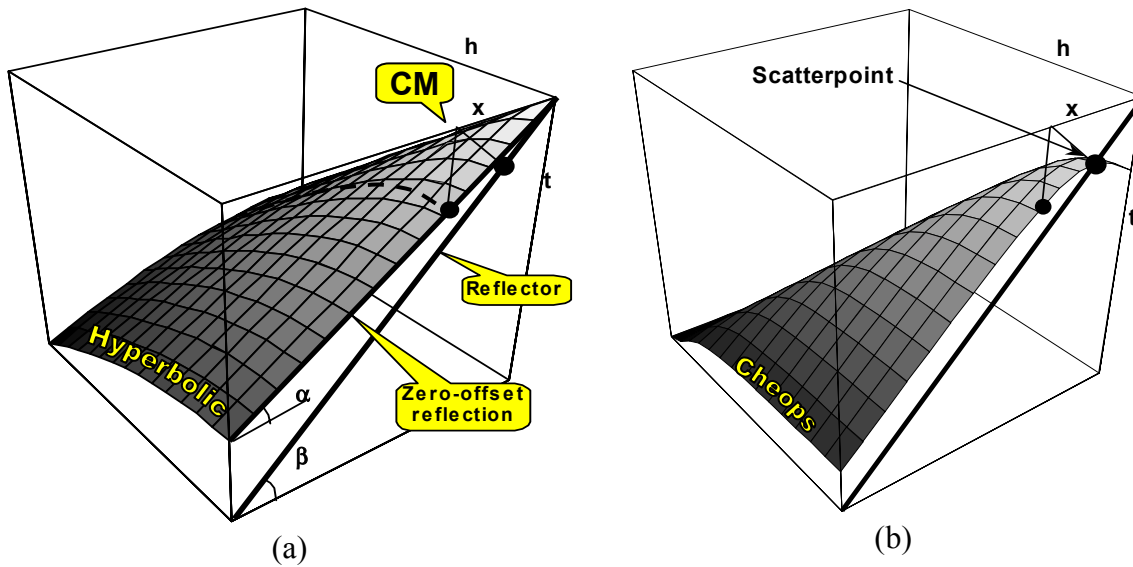


FIG 2. Dipping reflections illustrating in a) reflection times in a CMP gather, and b) the offset raypaths for a single reflection point (From Bancroft, 1999).

The surfaces in Figures 3 (a) and (b) are combined in (c) to illustrate the area of tangency between the dipping surface and Cheops' pyramid. The black line defines the theoretical tangency location while the gray band was formed by slightly reducing the time of Cheops' pyramid. As the offset is increased, the area of tangency curves down dip corresponding to that shown in Figure 2b. It is the energy in this tangency band that should be summed to the reflection point, i.e. pre-stack migration by summing over Cheops' pyramid.

Summing the hyperbolic energy in a CMP gather does not accomplish the same task, but smears the reflection point energy along the zero-offset dip.



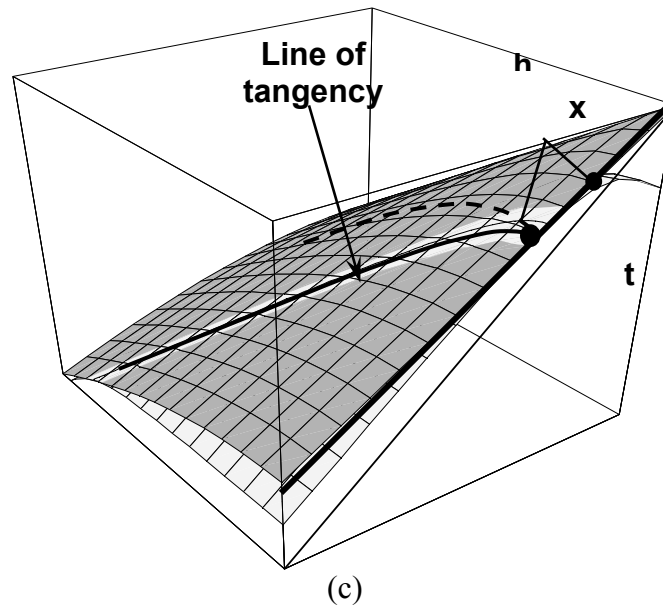


FIG 3. Dipping pre-stack surface from a series of scatterpoints and Cheops' pyramids, a) the dipping pre-stack surface, b) Cheops' pyramid from one scatterpoint, and c) a combination of (a) and (b) showing the line of tangency (From Bancroft, 1999).

### Equivalent offset and incident angle

As mentioned above, pre-stack migration moves the specular energy along the surface of Cheops' pyramid to reflection point or scatterpoint. The first step in the equivalent offset method (EOM) is to move the specular energy along Cheops' pyramid to form an equivalent hyperbola in a common scatterpoint (CSP) gather. To use this equivalent hyperbola as AVO analysis tool, the relationship between equivalent offset and incident angle must be investigated.

In forward modelling, the reflection energy from one reflection point on a horizontal reflector, i.e. specular energy, forms a hyperbola as a function of offset as shown in Figure 4 (the dark curve). The specular energy corresponds to the same traveltime band on a Cheops' pyramid travelled from a scatterpoint of the same location. Along the specular energy hyperbola, each point corresponds to each incident angle, which varies with half-offset  $h$ .

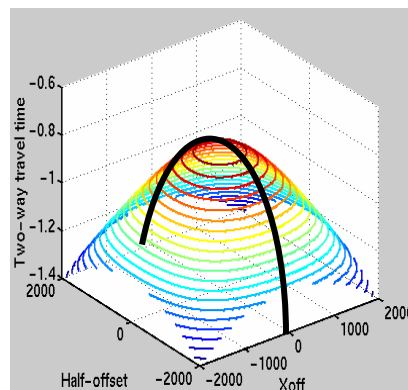


FIG 4. Reflection energy of one reflection point on a horizontal reflector in Cheops' pyramid is a hyperbola (the dark curve).

When forming a CSP gather, the energy on the surface of Cheops' pyramid becomes an equivalent hyperbola. The specular energy, i.e. the reflection energy, is moved to its corresponding position in the equivalent hyperbola. It varies with the incident angle or half source-receiver offset  $h$ . However the equivalent offset  $h_e$  is also a function of  $h$ . Therefore, the incident angle can be a function of  $h_e$  as equation (1) represents.

$$h_e^2(\theta) = h^2(\theta) + x_{off}^2 - \frac{4x_{off}^2 h^2(\theta)}{(VT(\theta))^2} \quad (1)$$

For a horizontal reflector, the apex of Cheops' pyramid corresponds to  $x_{off}$  is zero at the tangent point. In this case, the equivalent offset  $h_e$  equals half of the source-receiver offset  $h$  along the specular energy hyperbola. In a manner similar to the half-offset hyperbola, the incident angle varies with the equivalent offset as shown in the gray line of the curve in Figure 5b. The dash circle in Figures 5a and b shows the zero incident angle position in equivalent offset section. For a dipping reflector, the zero incident angle no longer corresponds with the apex of Cheops' pyramid, but to a position down along the equivalent hyperbola. The bold line in Figure 5a is for a dipping reflector. Angle of incidence with equivalent offset for a dipping reflector is shown in the lower side in Figure 5b, starting down in the hyperbola. The zero incident angle's position of a dipping reflector is shown by a solid circle.

Figure 5 also verifies that if there is only high frequency specular energy, the equivalent offset provides a one-to-one mapping of the incident angle to the CSP gather. This is the bridge between CSP gathers and amplitude analysis in CRP gathers.

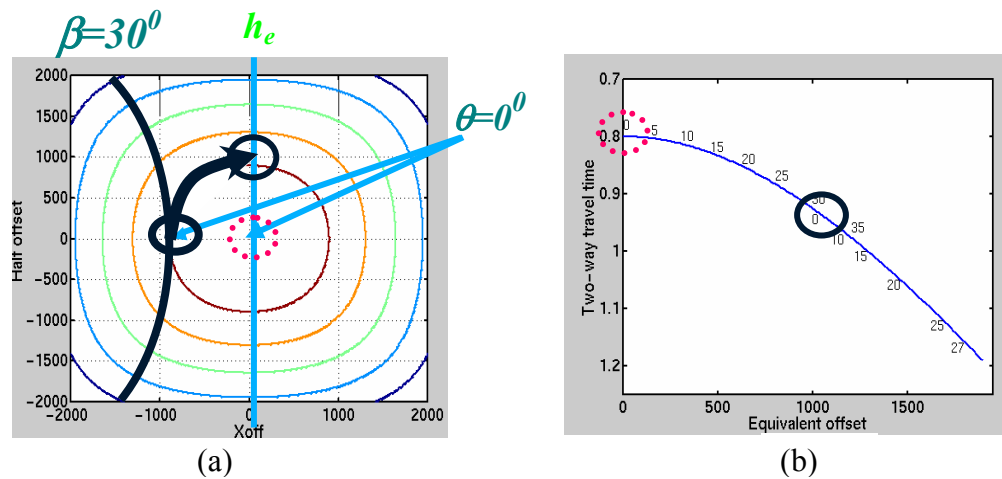


FIG 5. a) Contour of Cheops' pyramid relates to equivalent offset, dipping angle  $\beta$  and incident angle  $\theta$ ; b) relationship between equivalent offset and incident angle.

In forward modelling, the incident angle corresponds uniquely to equivalent offset. Actually CSP gathering is an inverse process, which starts from the equivalent offsets, and collects all possible energy to the CSP gather. In this direction, the energy moved to a certain equivalent offset position should correspond to a certain incident angle. The

relationship from equivalent offset to incident angle during CSP gathering must also be investigated to establish the uniqueness.

The CSP gathering is a mapping process from CMP to CSP. To realize the mapping, there are three loops as Figure 6 shows.

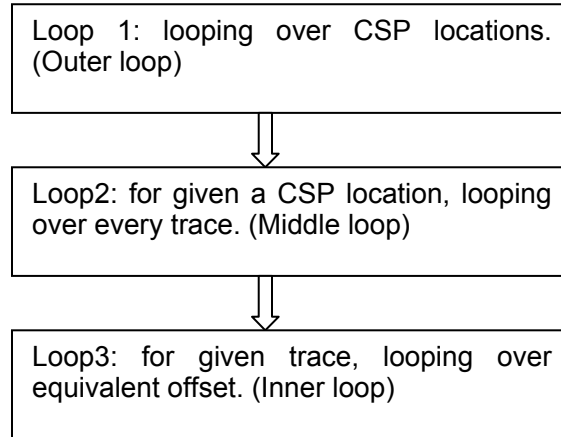


FIG 6. CSP gathering process loops.

For the given CSP location, first the equivalent offset should be defined using maximum traveltime and velocity information in the seismic section. Generally the equivalent offset is larger than half-offset but with the same interval. In doing this CSP gathering is naturally an anti-aliasing process (Bancroft et al, 1998). Then according to the trace information, calculate the CMP to CSP distance  $x_{off}$ , half-offset  $h$  and loop over every trace. Consequently loop over equivalent offset to collect energy to CSP gather. The whole CSP gathering is completed.

In a simple horizontal layer model, gathering along the Cheops' pyramid surface involves only moving the specular energy to the CSP gather. Corresponding to specular energy, the amplitude in the CSP gather should be the same as in the CMP gather. Forward modelling this simple subsurface structure, the surface CSP location is in the middle of the survey. But as Figure 7 shows, the CSP gather has several kinds of migration noise.

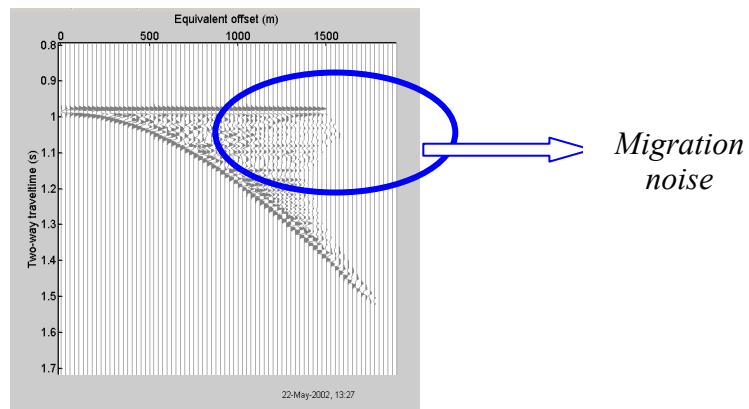


FIG 7. CSP gather with a lot of migration noise.

It is obvious that the CSP gather is not the same as the CMP gather, as Figure 8 shows the same position's CMP. The amplitude cannot be trusted. In order to search for the reason of migration noise, equation (1) may be evaluated in detail.

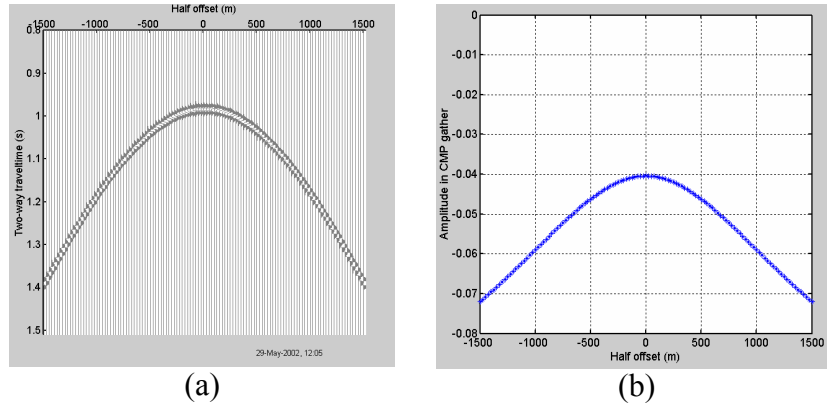


FIG 8. CMP gather at the same position as CSP gather: a)CMP gather; b)amplitude in CMP gather varies with half-offset.

According to equation (1), two factors,  $x_{off}$  and  $h$ , affect the equivalent offset  $h_e$ . Thus, whether the migration noise comes from these two factors will be investigated below.

*Smearing factor  $x_{off}$*

Equation (1) expresses the relationship between migration distance  $x_{off}$ , half-offset  $h$  and equivalent offset  $h_e$ . To examine the relationship between migration distance  $x_{off}$  and equivalent offset  $h_e$ , common offset gather with constant half-offset  $h$  is used to form the CSP gather. It is desired that for a given common offset gather the equivalent offset should be equal to half-offset. And the specular energy should appear in the same position in the equivalent hyperbola as in half-offset hyperbola. Figure 9 is the zero-offset section. Forming a CSP gather using this section, the results are displayed in Figure 10 in which Figure 10a is the CSP gather and 10b is the amplitude in the CSP gather.

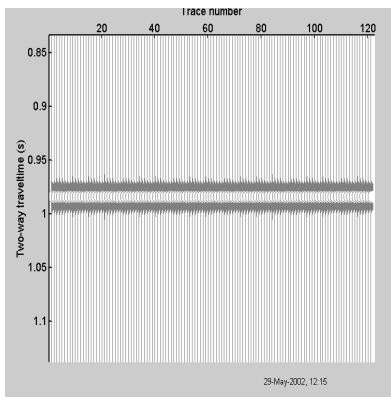


FIG 9. Zero-offset common offset section

Figure 10 indicates that the migration noise from migration distance  $x_{off}$  is obvious until the distance  $x_{off}$  reaches its maximum at the edge of the survey. This factor rises up the migration noise from the zero-offset data. Although the zero equivalent offset

corresponds to zero incident reflectivity, the others must be eliminated or otherwise they will destroy the whole CSP gather when the traveltime difference between the adjacent equivalent offset is smaller than a half period of the wavelet.

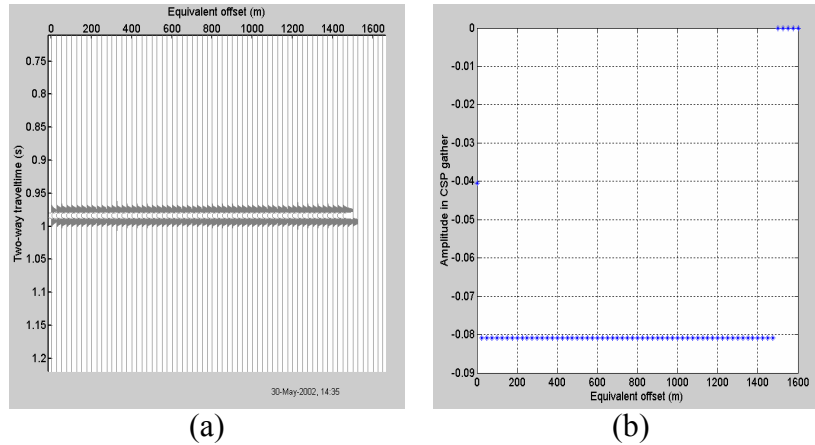


FIG 10. Forming CSP gather using zero-offset section. a) CSP gather; b) amplitude in CSP gather.

The zero-offset section contains the special data in a seismic survey. Generally Kirchhoff pre-stack migration is performed in a common-offset gather. Figure 11 is the common offset gather with half-offset  $500m$ . When forming a CSP gather using this section, as with the zero-offset section, the specular energy in the half-offset domain should be mapped to the same position as in the equivalent offset section and the amplitude should also be the same. Figure 12 shows the CSP gathering results.

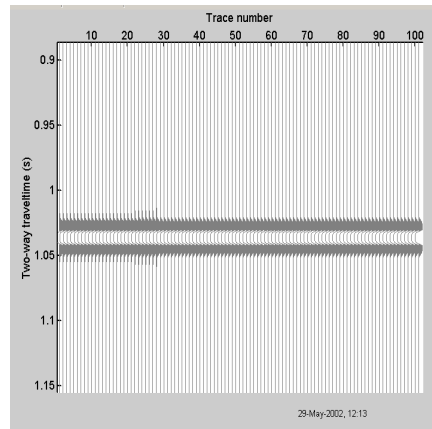


FIG 11. Common-offset gather with half-offset  $500m$ .

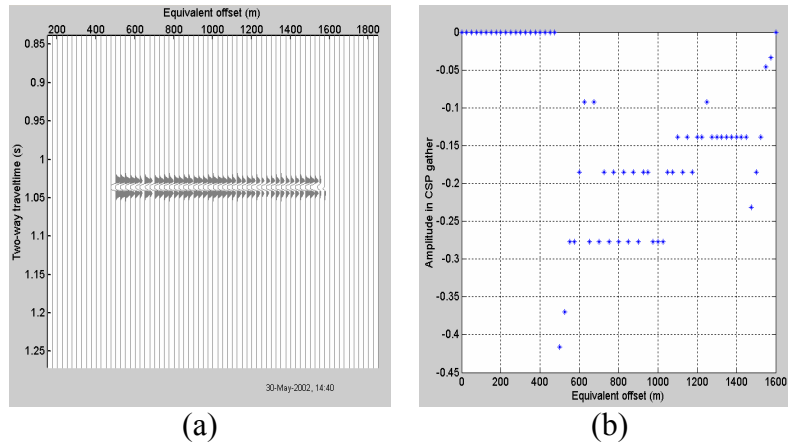


FIG 12. CSP gather using the data above. a) CSP gather; b) amplitude in CSP gather.

When compared with the CMP gather in Figure 8, the amplitude at equivalent offset  $500m$  is not the same as at half-offset  $500m$ . In the CSP gather, besides the amplitude error, migration distance  $x_{off}$  rises up a series of noisy traces which come from other traces with same half-offset.

For a linear reflector the reflected energy comes from the Fresnel zone centred at the tangent point. Using the Fresnel zone concept, the minimum migration aperture is obtained. Similar to the Kirchhoff common-offset migration algorithm, during the CSP gathering, the Fresnel zone can be used as the migration aperture. EOM with a limited migration aperture is named limited-aperture EOM. Here, one thing should be emphasized: EOM has the merit of high fold when used as imaging, but when used as an AVO analysis tool, the aperture should be limited. With a limited aperture, the migration signal is not only strong enough but also eliminates a lot of smearing from the migration distance. The results from zero-offset and common-offset data with limited aperture are depicted in the following pictures.

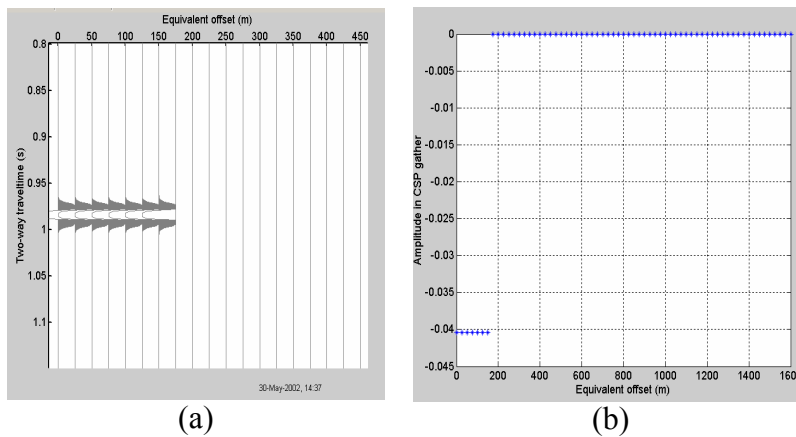


FIG 13. CSP gather using zero-offset data with limited aperture. a) CSP gather; b) amplitude in CSP gather.

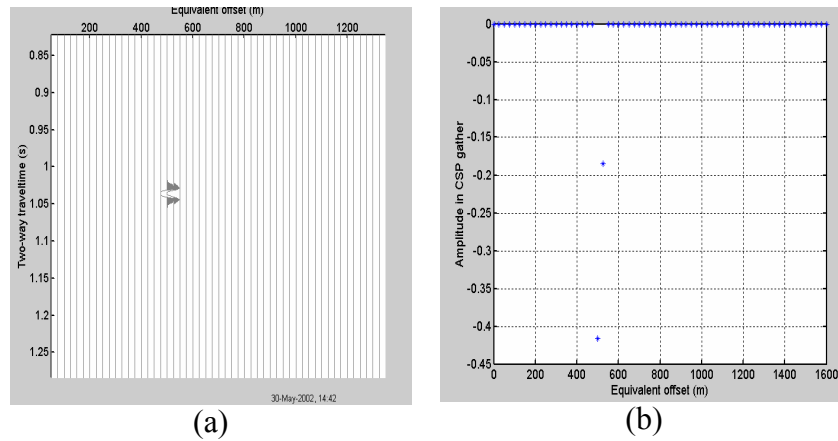


FIG 14. CSP gather using 500m offset section with limited aperture. a) CSP gather; b) amplitude in CSP gather.

The effect of a limited aperture’s improvement of the CSP gather is clearer in the 500m offset results. The smearing was reduced to two traces, of which one is at the correct position and the other is still migration noise. Is the signal lost during limiting the aperture? In both sections the amplitude in the CSP gather is larger than it should be. This verifies that within the limited aperture the energy is enough for energy collecting. When this method is tested with the whole data volume to form a CSP gather, comparing the result in Figure 15 to that with no limited aperture in Figure 7, the migration noise disappears dramatically. Only in the near equivalent offset is there still some migration noise left. In this sense limited-aperture CSP gathering clears part of the way for using CSP to get the reflectivity.

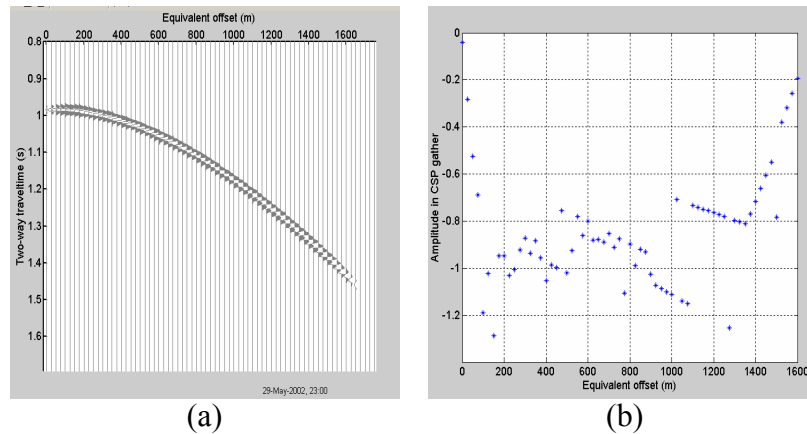


FIG 15. CSP gather with limited aperture formed using whole data. a) CSP gather; b) amplitude in CSP gather.

*Smearing factor  $h^2$*

Traditionally AVO analysis is performed in a CMP gather. In seismic survey the half-offset is defined in both positive and negative directions. The reflectivity of a single reflection point varies with half-offset in both directions in the same way. As half-offset becomes larger in this simple model, the reflectivity shows the obvious first class AVO anomalies. The AVO analysis needs only the one offset direction as Figure 16 shows.

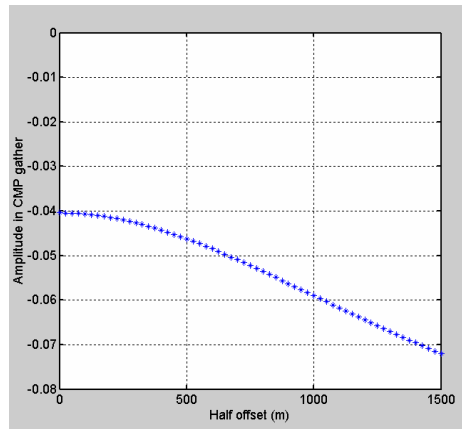


FIG 16. Amplitude varies with half-offset  $h$ .

Because, during CSP gathering, equivalent offset is calculated using  $h^2$ , both the positive and negative half-offset information are added to the same equivalent offset position. This square of half-offset leads to another smearing of amplitude in the CSP gather. To solve this smearing, it is necessary to form a two-sided CSP gather. To do so, a simple step of rearranging the positive half-offset information to positive equivalent offset direction and negative half-offset to negative equivalent offset is needed. After the rearranging, amplitude in the CSP gather is improved. The improvement in common-offset section is shown in Figure 17.

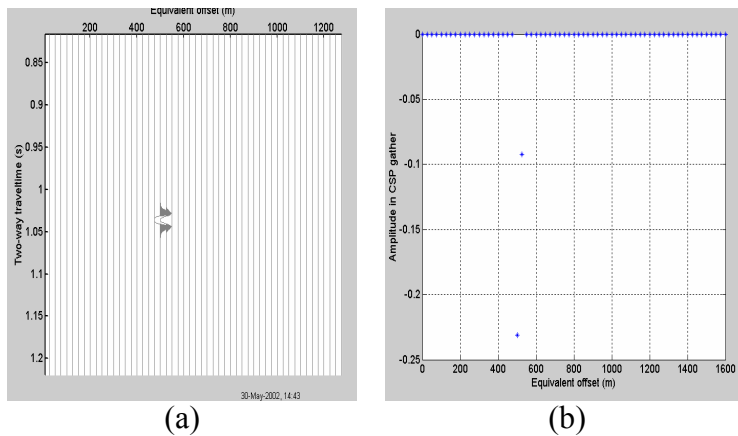


FIG 17. CSP gather formed using 500m half-offset section divided by fold of half-offset  $h$ . a) CSP gather; b) amplitude in CSP gather.

Using the whole data to form the CSP gather, the result is shown in Figure 18, which a) shows the CSP gather, b) shows the amplitude in CSP gather.

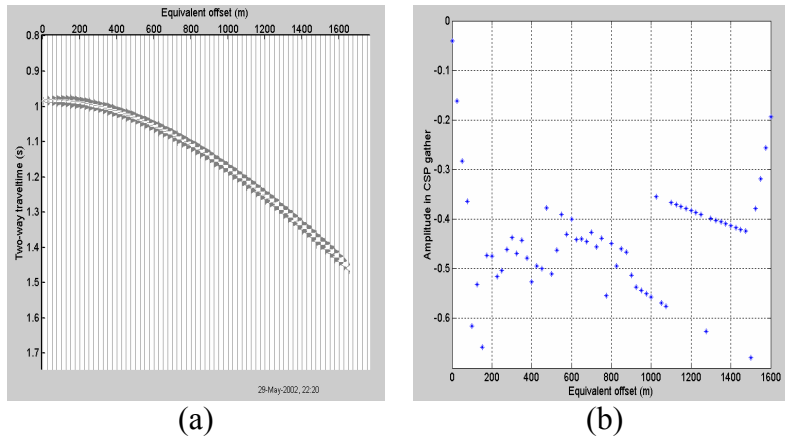


FIG 18. CSP gather using the whole data. a) CSP gather; b) amplitude in CSP gather.

In the above section the smearing factors were investigated and the solution was discussed. After eliminating all the smearing factors, the amplitude in a CSP gather isn't the reflectivity, and cannot show the amplitude anomalies. For analysis of this phenomena, a fold during CSP gathering is the first consideration.

**Fold consideration**

Fold is considered as a possible reason for larger amplitude, besides smearing factors. In CSP gathering, fold can be calculated sample by sample. Due to the survey geometry, the fold becomes larger with the equivalent offset. A normally divided CSP gather by fold provides a chance to correct amplitude in the CSP gather.

Figure 19 shows the example of a CSP gather divided by sample-by-sample fold with a migration aperture Fresnel zone. Upon observation of the amplitude in the CSP gather in Figure 19b, it is obvious that the amplitude in CSP gather has been too divided compared to the amplitude in the CMP gather.

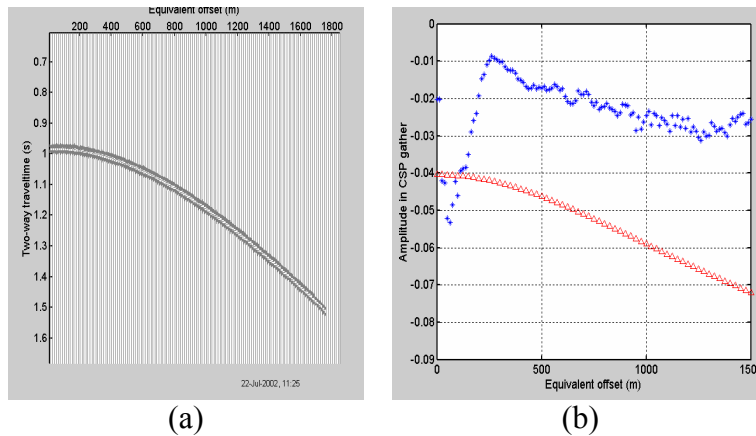


FIG 19. CSP gather divided by fold with Fresnel zone as aperture. a) CSP gather; b) amplitude in CSP gather.

Because during CSP gathering the energy, which has been collected to the CSP gather each time, is not completely the reflection energy, some of the energy is far smaller than the reflection energy. But fold is calculated each time no matter what part of the energy adds to the CSP gather. Based on such consideration, a smaller aperture, such

as half the Fresnel zone will be tested. A limited migration aperture to half the Fresnel zone means that not only is the energy within the aperture mainly reflection energy but also fold calculation can be more reliable. Figure 20 shows the plausible results compared with reflectivity indicated by triangles in Figure 20b.

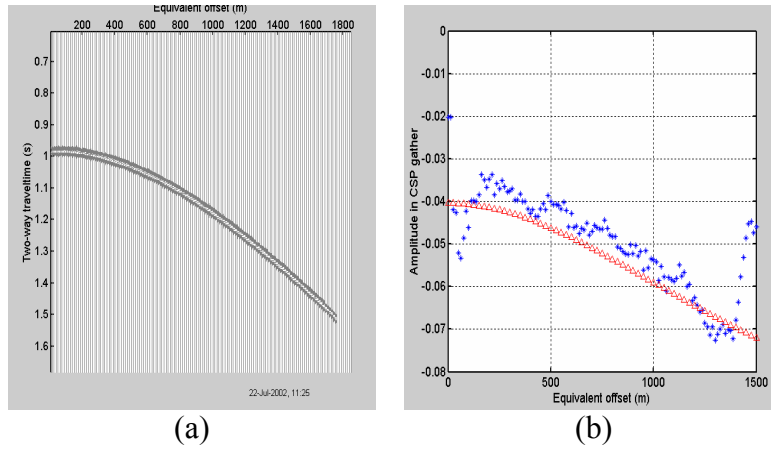


FIG 20. CSP gather divided by fold with half the Fresnel zone as aperture. a) CSP gather; b) amplitude in CSP gather.

With half the Fresnel zone as migration aperture and divided by sample-by-sample fold, the amplitude in the CSP gather approximates reflectivity. This is the first kind of approach for a CSP gather to be used as an amplitude analysis tool.

For prestack Kirchhoff migration, many geophysicists have recently devoted themselves to the development of a true-amplitude migration algorithm for AVO analysis after prestack migration, which provides greater correcting subsurface imaging. In these literatures, to achieve true-amplitude migration, the weighting function or scaling factor, which is used in this paper, is the most important factor. The reason in this paper for using a scaling factor is that the scaling factor does not take into consideration any effect from the geometric spreading, transmission lose or wavelet. In the next section, different scaling factors will be discussed and tested using the same simple model as above.

### Scaling factors during CSP gathering

#### *Margrave's approach*

Margrave (et al., 1999) first introduced the Fourier prestack migration by equivalent wavenumber (EWM). He also evaluated the time migration EOM's scaling factor. In the next several pages, his EWM method and time scaling factor approximated from EWM will be introduced in detail.

Margrave (et al., 1999) began this derivation from Stolt prestack wavefield construction as:

$$\psi(x, h = 0, t = 0, z) = \iiint \phi_0(k_x, k_h, \omega) \exp(ik_z z) \exp(ik_x x) dk_x dk_h d\omega, \quad (2)$$

In equation 2 the Fourier double square root can be rewritten as a single square root involving an equivalent wavenumber. The equivalent wavenumber  $k_e$  can be expressed implicitly as:

$$k_z = \frac{1}{2}\sqrt{k^2 - (k_x - k_h)^2} + \frac{1}{2}\sqrt{k^2 - (k_x + k_h)^2} = \sqrt{k^2 - k_e^2}, \quad (3)$$

where  $k=2\omega/v$ .

The algebraic solution for  $k_e$  is

$$k_e^2 = k_x^2 + k_h^2 + \frac{k_x^2 k_h^2}{k_z^2} = \frac{1}{2}(k_x^2 + k_h^2 + k^2) - \frac{1}{2}\sqrt{(k^2 - k_x^2 - k_h^2)^2 - 4k_h^2 k_x^2}. \quad (4)$$

Changing the variables in equation (4) from  $(k_x, k_h, k)$  to  $(k_x, k_e, k)$ , results in

$$\psi(x, h = 0, t = 0, z) = \frac{v}{2} \iint \bar{\phi}(x, k_e, k) \exp(iz\sqrt{k^2 - k_e^2}) dk_e dk, \quad (5)$$

where

$$\bar{\phi}(x, k_e, k) = \int f(k_x, k_e, k) \phi_0(k_x, k_h, k) \exp(ik_x x) dk_x, \quad (6)$$

and

$$f(k_x, k_e, k) = \frac{k_e}{k_h(k_e)} \left[ 1 - \frac{k_e^2 - k_h^2(k_e)}{k^2 + k_x^2 - k_e^2} \right], \quad (7)$$

with

$$k_h(k_e) = \text{sign}(k_e) \sqrt{\frac{[k^2 - k_e^2][k_e^2 - k_x^2]}{k^2 - k_e^2 + k_x^2}}. \quad (8)$$

Since

$$\sin(\theta_x) = \frac{k_x}{k} = \frac{2(x-x_0)}{vT}; \quad \sin(\theta_h) = \frac{k_h}{k} = \frac{2h}{vT}; \quad \sin(\theta_e) = \frac{k_e}{k} = \frac{2h_e}{vT}, \quad (9)$$

then the scale function  $f$  can be written in space-time domain as

$$f = \frac{\sin(\theta_e)}{\sin(\theta_h)} \left( 1 - \frac{\sin^2(\theta_e) - \sin^2(\theta_h)}{1 + \sin^2(\theta_x) - \sin^2(\theta_e)} \right). \quad (10)$$

Using equation 10 as the scaling factor together with the Fresnel zone as aperture, the result shows that except in near offset, there are several singular points. The other amplitudes in the equivalent hyperbola are ideal as reflectivity.

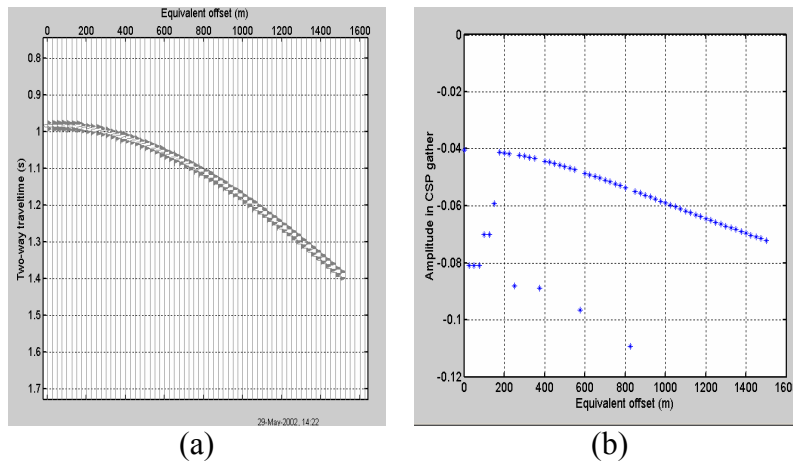


FIG 21. CSP gather using scaling factor from EWM. a) CSP gather; b) amplitude in CSP gather.

*Scaling by aperture normalization*

This idea comes from scaling that uses aperture normalization. The basic idea is amplitude scaling by the ratio between migration aperture and migration distance  $x_{off}$ . In the next part two considerations will be used for CSP gathering.

*1. Linear approach:  $1-x_{off}/x_{aper}$*

Linear approach scaling factor  $1-x_{off}/x_{aper}$  is first considered as a scaling factor during the CSP gathering, where  $x_{aper}$  denotes the migration aperture and  $x_{off}$  denotes the migration distance. With limited migration aperture to Fresnel zone using this linear approach, amplitude anomalies are clear in the CSP gather, but it is not the reflectivity. Thus scaling using this method cannot provide correct amplitude after CSP gathering.

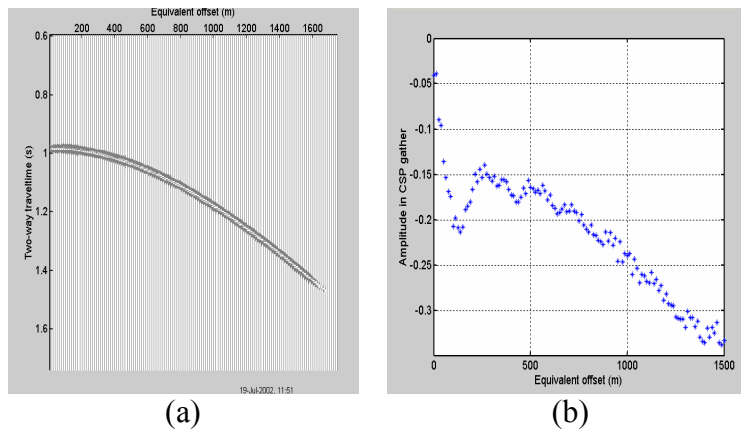


FIG 22. CSP gather uses linear approach of aperture normalization. a) CSP gather; b) amplitude in CSP gather.

A limited aperture to half the Fresnel zone, as discussed in the fold consideration section, using the linear approach amplitude in the CSP gather, does not show improvement (Figure 23). Also, enlarging the migration aperture to double the Fresnel zone does not improve the amplitude, which is described in Figure 24.

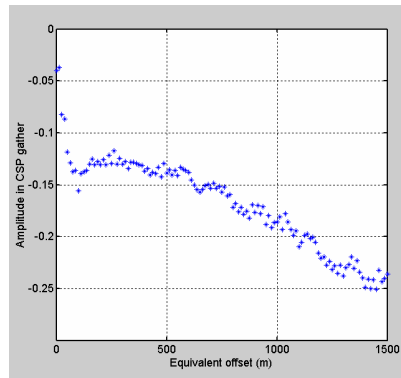


FIG 23. CSP gather scaled using linear approach with half the Fresnel zone as aperture.

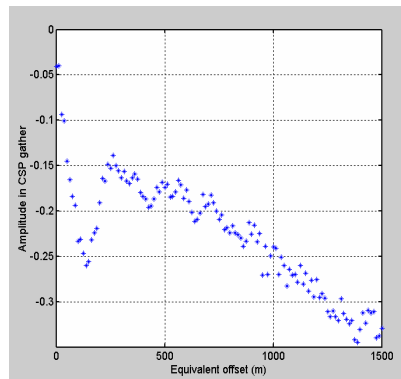


FIG 24. CSP gather scaled using linear approach with double the Fresnel zone as aperture.

## 2. Exponential approach: $0.25 * e^{(-x_{\text{off}} / x_{\text{aper}})}$

The third approach to aperture normalization is called the exponential approach, i.e.  $0.25 * e^{(-x_{\text{off}} / x_{\text{aper}})}$ . The exponential approach comes from diffraction theory. The amplitude decreases dramatically within the Fresnel zone with the distance to the edge of the reflector. The exponential approach approximates that the amplitude decreases with migration distance to migration aperture exponent.

First, Fresnel zone size is used as the migration aperture. As Figure 25 shows, amplitude in the CSP gather not only indicates the amplitude anomalies but also approximates the reflectivity, in which reflectivity is shown by triangles.

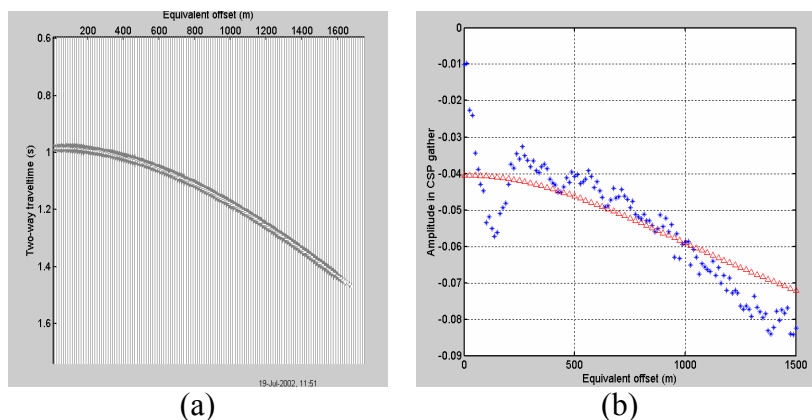


FIG 25. CSP gather uses exponential approach of aperture normalization. a) CSP gather; b) amplitude in CSP gather.

With the test above, the migration aperture is now limited to half the Fresnel zone. The results are shown in Figure 26. Amplitude in this circumstance has a little improvement over the last case. It approximates reflectivity too.

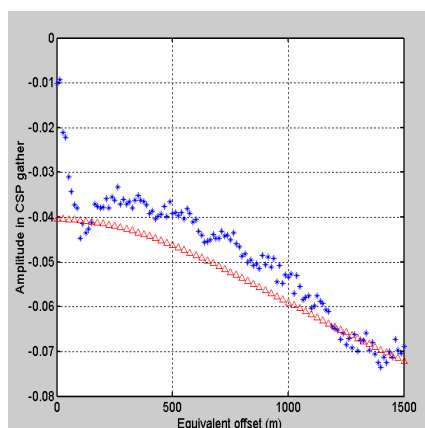


FIG 26. CSP gather scaled using exponential approach with half the Fresnel zone as aperture.

Testing the method using double the Fresnel zone as aperture provides same results as Figure 27 shows.

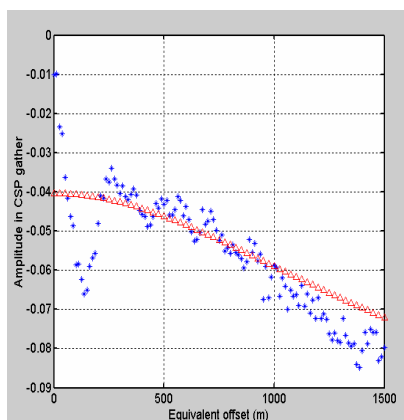


FIG 27. CSP gather scaled using exponential approach with double the Fresnel zone as aperture.

## EXAMPLE

### Earth model and acquisition geometry

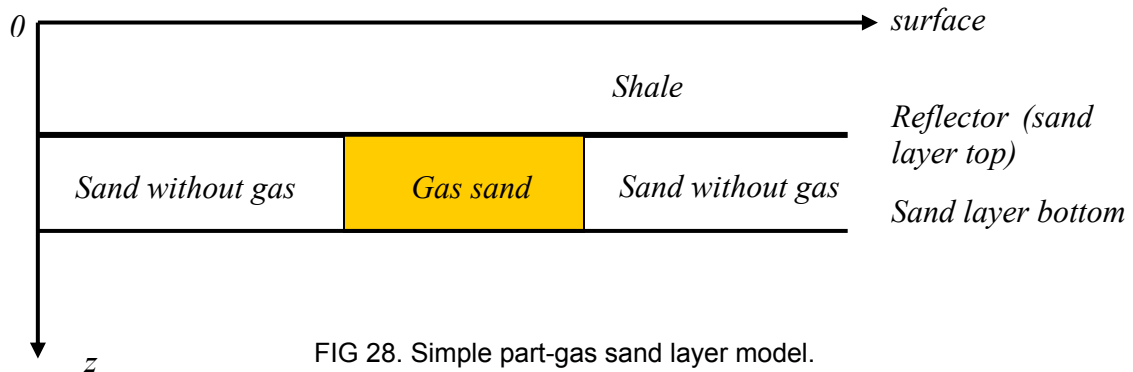
The experiments presented in this part are based on the simple earth model, called the part-gas sand layer model, as shown in Figure 28. The earth properties are:

P-wave velocities: in Shale  $3048\text{m/s}$ , in sand (with gas and without gas)  $2438\text{m/s}$ ;

S-wave velocities: in Shale  $1244\text{m/s}$ , in sand without gas  $995\text{m/s}$ , in sand with gas  $1625\text{m/s}$ ;

Densities: in Shale  $2.4\text{g/cm}^3$ , in sand (with gas and without gas)  $2.14\text{g/cm}^3$ .

According to the Zoeppritz equation, when a P-wave travels through the subsurface with these earth parameters, the seismic section splits into two parts. With the gas sand, there are strong AVO anomalies, gasless sand there is no such phenomena.



A synthetic dataset is generated. The survey geometry is illustrated in Figure 29. In this survey, sources and receivers are located on the surface. Receivers are fixed from  $0$  to  $4000$  at  $25\text{m}$  intervals. Sources move along the surface from  $500\text{m}$  to  $3500\text{m}$  also at  $25\text{m}$  intervals. This geometry creates pre-stack data with fold up to  $121$  high.

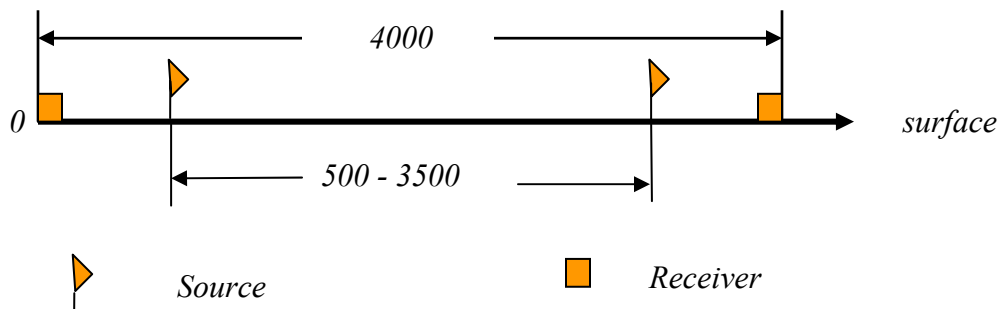


FIG 29. Geometry used to acquire a set of data over the earth subsurface model shown in Figure 28.

The synthetic seismic data is numerically generated using MatLab, in which the reflection coefficients calculated by Aki and Richards' approximation to the Zoeppritz

equation was convolved with the Ricker wavelet with a dominant frequency at 50hz. Time sample rate is 2 milliseconds. Only the primary P-P reflection was modelled.

### AVO analyses in CMP gathers for gas sand

For the horizontal layer, AVO analysis in the CMP gather traditionally provides reliable amplitude information. For example, when the CMP is located within the gas sand, surface location at 1800m, the first kind of AVO anomalies is expected, as Figure 30 shows.

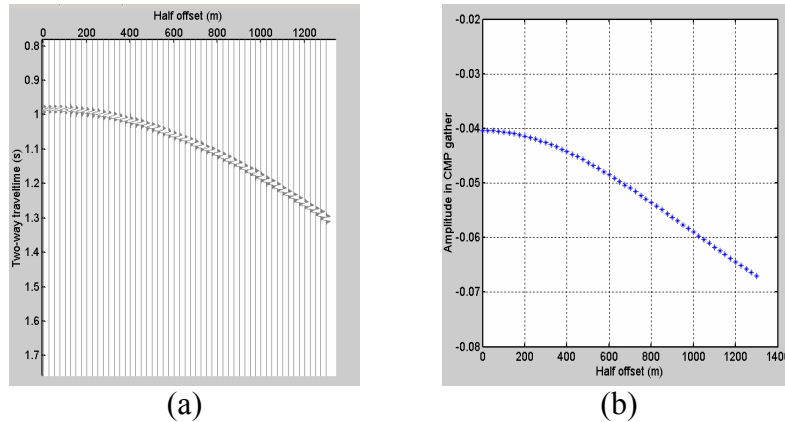


FIG 30. CMP gather within gas sand. a) Seismic section; b) amplitude varies with half-offset.

For this classic gas-sand model, reflection coefficients become smaller when the half-offset is larger or the incident angle is larger. The reflection coefficients are negative and become more negative. Half-offset  $h$  varies from 0 to 1300 metres. Amplitudes, which are reflection coefficients convolved with the Ricker wavelet, vary from  $-0.04$  to  $-0.068$ ; the trough becomes dramatically larger with half-offset  $h$ .

### AVO analyses in CSP gathers for gas sand

As obtained in the above section, there are three approaches in getting correct amplitude in CSP gathers. Now the three approaches will be applied to synthetic data separately.

*First approach: half the Fresnel zone as aperture divided by fold*

From a CSP gather in the same position as the CMP gather using the first kind of approach, Figure 31 represents the result, in which (a) shows the image CSP gather and (b) shows the amplitude in such a gather. The triangles represent amplitude in the CMP gather, which is reflectivity convolved with the wavelet. Amplitude in the CSP gather is a good fit to the reflectivity in this circumstance.

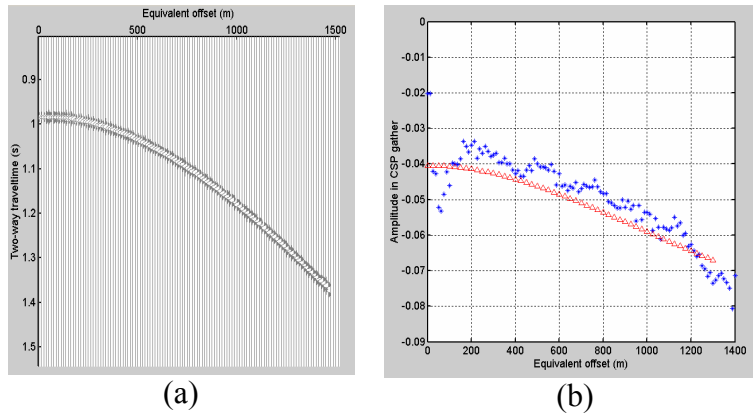


FIG 31. CSP gather formed using first approach in gas-sand area. a) CSP seismic section; b) amplitude in such gather.

*Second approach: Fresnel zone as aperture with scaling factor EWM's*

The CSP gather with a limited aperture and EWM's scaling factor can provide the correct amplitude. To verify the reliability of the amplitude in the CSP gather, the method is directly used to generate a CSP gather with the same location as the CMP. The amplitude in the CSP gather is as expected. The results are shown in Figure 32.

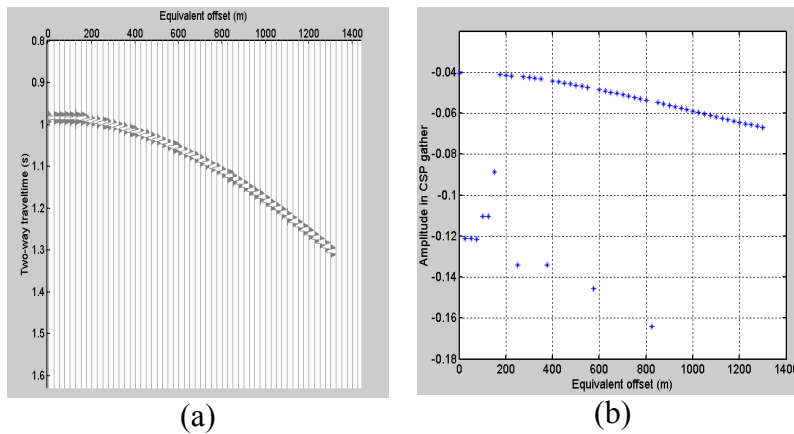


FIG 32. CSP gather is formed using EWM's approach in gas-sand area. a) CSP seismic section; b) amplitudes in CSP gather.

In the amplitude picture, there are several singular points with extremely large amplitudes at the near equivalent offset. The rest of it is the same as the CMP gather's amplitude. Detailed comparisons are illustrated next.

With the closely compared amplitudes in the CSP and CMP gathers, the extreme points were abandoned. Because this model is a horizontal reflector in the subsurface, the equivalent offset  $h_e$  should equal to the half-offset  $h$ . Figure 33 shows that they are exactly identical. The amplitude in these two different gathers are identical, both vary with the offset and become larger.

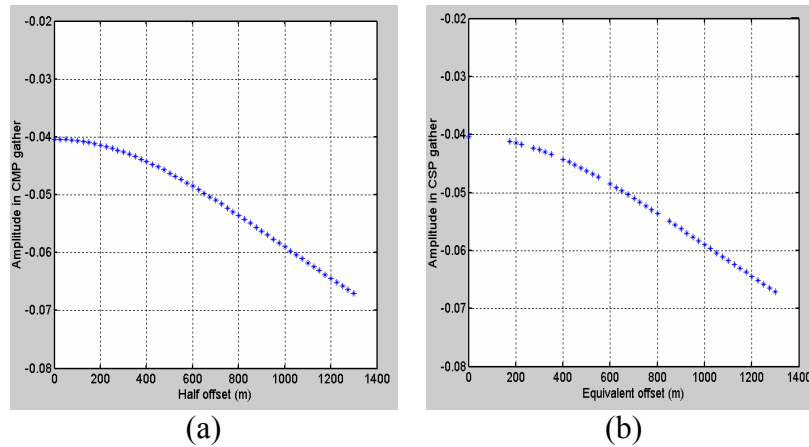


FIG 33. Close comparison of the amplitude in CMP and CSP gather. A) Amplitude in CMP gather; b) amplitude in CSP gather without the extreme larger near offset points.

*Third approach: Fresnel zone as aperture with aperture exponential scaling*

The CSP gather formed using the exponential scaling of aperture can also provide a good fit to reflectivity. Figure 34 shows the results. In the CSP gather the amplitude shows a perfect anomaly trend, coincident with the CMP gather, which is in triangles.

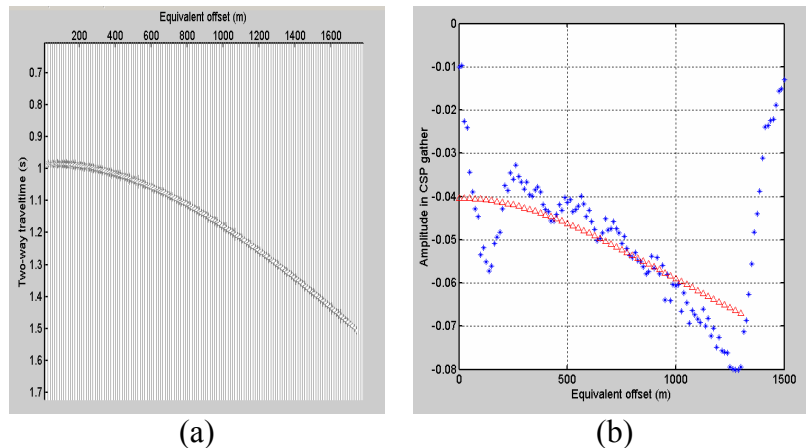


FIG 34. CSP gather is formed using exponential approach. a) CSP gather; b) amplitude in CSP gather.

In summary, the three approaches applied to this simple model can provide the correct amplitude in gas-sand area. To verify these, the next application is to gasless sand areas, in which no amplitude anomaly will be detected.

**AVO analyses in CMP gather for gasless sand**

In this synthetic data, besides the central gas sand section, the rest of the lower layer is gasless sand. For reflection from Shale to gasless sand, the reflection coefficients are still negative but do not become more negative with the incident angle. The reflection coefficient of normal incidence is the same as from Shale to gas sand. The reflection coefficients of angle incidence remain almost the same, and a little bit larger.

The same procedure used to generate the CMP gather for this gasless sand model is described in Figure 35. The amplitude in the CMP gather is described as well. The CMP locates in the surface at 2500 m.

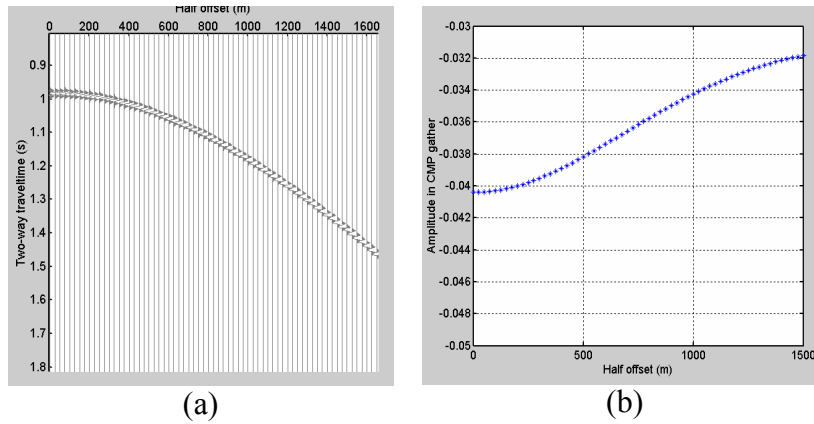


FIG 35. CMP gather shows amplitude for gasless model. A) CMP gather at surface location 2500m; b) amplitude in CMP gather.

Amplitude in this CMP section has an upward tendency. It varies from  $-0.04$  to  $-0.032$  with half-offset varying from 0 to 1500 m.

### AVO analyses in CSP gather for gasless sand

The limited aperture CSP gathering will be applied to form CSP gather at the surface location 2500m, which is within the gasless model.

*First approach: half the Fresnel zone as aperture and dividing by fold*

In the gasless sand area, amplitude in CSP gather with first approach is shown in Figure 36. Although the trend of amplitude is not easy to detect, the amplitude remains at the same level and it fits the amplitude in the CMP gather well.

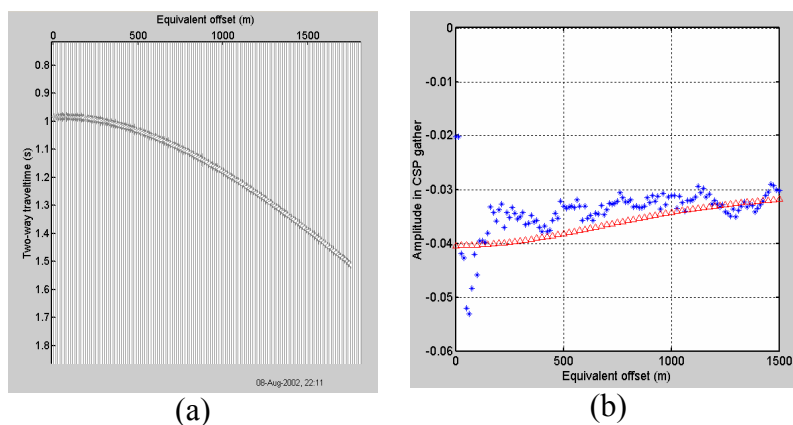


FIG 36. CSP gather is formed using first approach in gasless sand area. A) CSP gather; b) amplitude in CSP gather.

*Second approach: Fresnel zone as aperture with scaling factor EWM's*

The amplitude and CSP section using EWM's approach are shown in Figures 37, which (a) shows the CSP section and (b) shows the amplitude in the CSP gather.

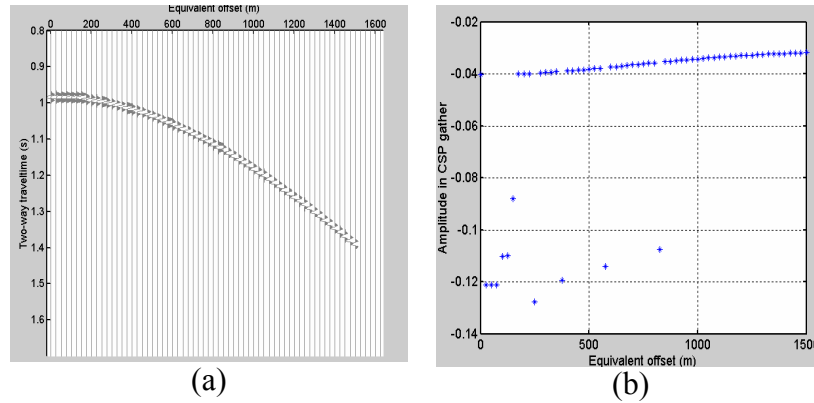


FIG 37. CSP gather is formed using EWM's approach in gasless sand area. a)CSP seismic section; b) amplitude in CSP gather.

There are several points of extreme amplitude in the near equivalent offset. Besides these singular points, the rest of the amplitude is the same as in the CMP gather. Close comparisons will be illustrated next.

Amplitude in the gasless model, as Figure 35 shows, varies from  $-0.04$  to  $-0.032$ . Thus the trough becomes smaller with half-offset  $h$ . Again, the extreme larger points are abandoned in CSP gather. Closely compared, the amplitude in the CMP gather and the CSP gather, as shown in Figure 38, are the same. This result verifies that the CSP gather can provide reliable amplitude or reflectivity whether there are AVO anomalies or not.

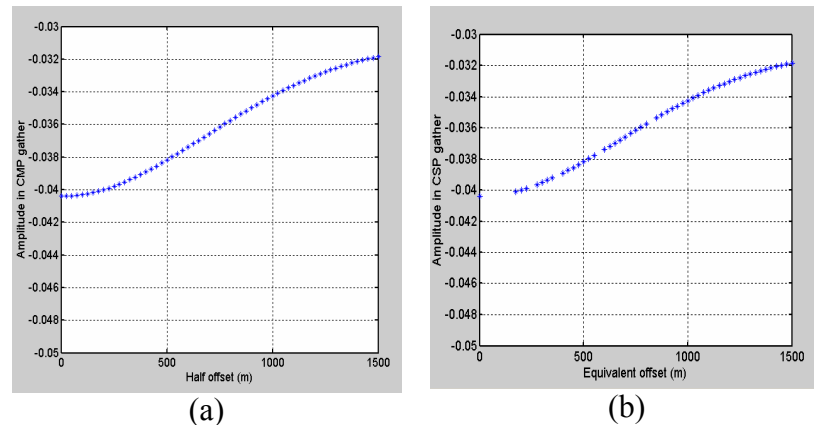


FIG 38. Comparison of amplitude in CMP gather and CSP gather without extreme points at the near equivalent offset: a) Amplitude in CMP gather; b) amplitude in CSP gather without the extreme points.

*Third approach: Fresnel zone as aperture with aperture exponential scaling*

The CSP gather is formed using aperture exponential scaling, and Figure 39 represents the results. Amplitude in the CSP gather remains at the same level and it fits the amplitude in the CMP gather well, except that the near equivalent offset amplitude in the CSP gather is larger than it should be. Figure 39 (b) verifies that exponential scaling

can provide correct amplitude with no amplitude anomaly as well as with amplitude anomaly.

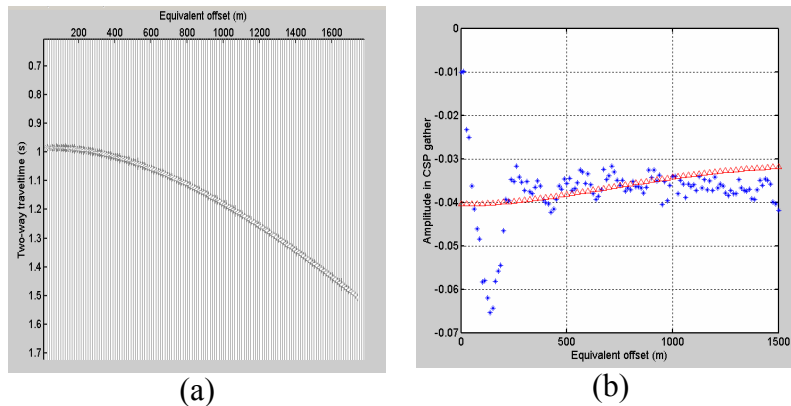


FIG 39. CSP gather is formed using exponential approach in gasless sand area: a) CSP seismic section; b) amplitude in CSP gather.

In summary, approaches using half the Fresnel zone aperture divided by fold and aperture exponential scaling to form the CSP gather can obtain the correct amplitude. The EWM's approach provides perfect amplitude in the CSP gather except for some singular points. Thus the three approaches can be used for CSP gathering as an AVO analysis tool after prestack migration.

## CONCLUSIONS

In summary, this paper discussed two smearing factors during CSP gathering:

- migration distance  $x_{off}$ ,
- square of half-offset  $h$  when calculating equivalent offset  $h_e$ .

With the elimination of smearing effects and division of the CSP gather by sample-by-sample fold with the half the Fresnel zone aperture, amplitude in the CSP gather approaches the reflectivity. In this paper this is called the first kind of approach to obtain reflectivity in the CSP gather.

During CSP gathering with EWM's scaling factor, the amplitude in the CSP gather is reflectivity. This is the second kind of approach.

Another good approximation of scaling during CSP gathering was introduced: exponential scaling within the Fresnel zone. Results show it can provide reflectivity in a CSP gather no matter what size of aperture is used. This is the third approach.

The synthetic data has two amplitude phenomena, one with the AVO anomaly and the other without. The results show that the amplitude in the CSP gather is the reflectivity, and provide reliable amplitude information.

## REFERENCES

- Aki, K. and Richards, P. G., 1980, Quantitative seismology theory and methods.
- Clarebout, 1985, Imaging the earth interior: SEG.
- Bancroft, J.C., 1998a, Dip limits on pre- and poststack Kirchhoff migrations: CREWES Project Research Report, 9, Ch.25.
- Bancroft, J.C., 1998b, Computational speed of EOM relative to standard Kirchhoff Migration: CREWES Project Research Report, 9, Ch.43.
- Bancroft, J.C., 1998c, Optimum CSP gathers with fixed equivalent offset: CREWES Project Research Report, 9, Ch.44.
- Bancroft, J.C. Geiger,H.D. and Margrave, G.F., 1998, The equivalent offset method of Prestack time migration: Geophysics, 63, 2042-2053
- Bancroft, J.C., and Xu,Y., 1998, Equivalent offset migration for vertical receiver arrays: CREWES Project Research Report, 9, Ch.29.
- Castagna, J.P. and Backus, M.M., 1997, Offset-dependent reflectivity-theory and practice Of AVO analysis: SEG No.8.
- Margrave, G. F., Bancroft, J. C. and Geiger, H. D., 1999,Fourier prestack migration by equivalent wavenumber: Geophysics,64,197-207.
- Ostrander, W.J., 1982, Method for interpretation of seismic records to yield indication of Gaseous hydrocarbons: United States Patent No.4316268.
- Sheriff, R.E. and Geldart, L. P., 1995, Exploration Seismology: Cambridge University Press.
- Sheriff, R.E., 1980, Nomogram for Fresnel-zone calculation: Geophysics, V 45, P. 968-972.

## ACKNOWLEDGEMENTS

We thank the sponsors of the CREWES project and NSERC for supporting this research.